Proceedings of the Thirty-sixth (2026) International Ocean and Polar Engineering Conference www.isope.org
Orlando, Florida, USA, May 31-June 5, 2026

ISBN 978-1-880653-72-2; ISSN 1098-6189

Numerical Investigation on the Underwater Space Spiral Maneuver of a Generic Submarine

Yuheng Sun[1], Jie Zhu[2], Liushuai Cao[1], Decheng Wan[1]*

[1] Computational Marine Hydrodynamics Lab (CMHL), School of Ocean and Civil Engineering,
Shanghai Jiao Tong University, Shanghai, China
[2] Wuhan Second Ship Design and Research Institute, Wuhan, China
*Corresponding Author

ABSTRACT

Submarine maneuvering motions typically involve a range of rotational actions, which are primarily intended to support tactical evasion and enhance a submarine’s operational agility. Among them, the space spiral maneuver is a key control action that enables the execution of complex maneuvering commands in an underwater environment. In this study, a Joubert BB2 submarine fitted with a Marine 7371R propeller is investigated by solving the Reynolds-averaged Navier–Stokes (RANS) equations coupled with the SST *k-ω* turbulence model to capture turbulent flows. To ensure numerical accuracy, a mesh-convergence study is performed using three levels of mesh resolution. An overset mesh approach is adopted to prescribe the motions of the submarine and its X-rudders, while a sliding mesh method is employed to model propeller rotation. The autopilot is implemented as a PD controller to automatically regulate the vehicle attitude. The results demonstrate that, under autopilot control, the submarine can enter a stable space spiral maneuver state. Moreover, because the deflection of each X-rudder plane can simultaneously induce vertical motion and turning, both the lift distance and turning radius increase with increasing vertical command. In addition, the study examines the effects of the space spiral maneuver on the hydrodynamic loads, pressure distribution, and vortical structures.

KEY WORDS: Computational fluid dynamics; Submarine; RANS; Overset Mesh; Space Spiral Maneuver.

INTRODUCTION

As a representative strategic asset in major-power military competition, a submarine’s maneuvering performance is not only a primary metric for assessing its tactical flexibility and battlefield survivability, but also a fundamental prerequisite for accomplishing missions such as strategic deterrence, covert penetration, and precision strikes under complex sea states. Consequently, research on the key performance indices governing submarine maneuverability is of substantial engineering significance and is strongly motivated by pressing practical demands.(Cao et al., 2023)

Currently, research on submarine maneuverability is primarily conducted through two approaches: experimental studies and numerical simulations. For full-body submarine models, several scholars have conducted maneuverability experiments in towing tanks. Liu et al. (Liu et al.) performed a maneuverability study on the DARPA SUBOFF model, providing comprehensive simulation data and detailed hydrodynamic data. Özden et al.(Özden et al., 2019) conducted self-propulsion model experiments on the SUBOFF submarine configuration in conjunction with the corresponding INSEAN E1619 propeller. Furthermore, Overpelt et al. (Overpelt et al.) carried out a series of experiments on the Joubert BB2 submarine model at the Marine Pool in the Netherlands. These experiments included resistance measurements for the bare hull, propeller open-water tests, self-propulsion tests, steady turning tests, and Zigzag maneuvering tests. Detailed hydrodynamic data and six-degree-of-freedom motion response data for the submarine were also provided. Lin et al. (Lin et al., 2023) conducted comparative analyses through model experiments to assess the hydrodynamic performance, maneuvering characteristics, and wake field quality of the submarine's cruciform rudder and X-rudders. These experimental studies provide foundational data and crucial references for the further understanding and optimization of submarine maneuverability.

With the continued advances in computational fluid dynamics (CFD), including the refinement of turbulence closures and the rapid growth of high-performance computing capability, numerical approaches can now provide reasonably accurate predictions of submarine maneuvering performance and offer practical guidance for real operations. In CFD-based studies of underwater-vehicle maneuverability, one major task is to couple the propeller with the vehicle to achieve a steady self-propelled condition, i.e., to perform self-propulsion maneuvering simulations. Dorgul et al. (Dogrul et al., 2017) simulated the deep-water self-propulsion performance of the SUBOFF model using a RANS approach. Lungu (Lungu, 2022) employed a detached-eddy simulation (DES) framework to investigate near-surface self-propulsion maneuvering of SUBOFF at three different submergence depths; the study quantified the hull resistance characteristics at different speeds and the open-water performance of the propeller, and further resolved the free-surface-induced variations in propeller performance together with the associated wave-pattern features. Chase et al. (Chase, 2012) applied an overset mesh technique to model propeller rotation during self-propulsion, enabling higher-fidelity resolution of the unsteady flow field associated with the rotating propulsor. Fossen et al. (Fossen and Blanke, 2000) proposed a velocity-based PI controller for self-propulsion prediction, in which the propeller rotational speed is adjusted via proportional–integral control at each time step to automatically converge to the self-propulsion point at a prescribed speed; this strategy remains one of the most widely adopted numerical procedures for determining self-propulsion points.

Building upon self-propulsion maneuvering simulations, increasing attention has been directed toward predicting submarines' more complex maneuvering behaviors. Carrica et al. (Carrica et al., 2021), using their in-house overset-mesh CFD solver REX, investigated the hydrodynamic performance of a submarine–propeller system and simulated six-degree-of-freedom (6-DOF) turning and Zigzag maneuvering motions under both calm-water and wave conditions. Chen et al. (Chen et al., 2023) combined a dynamic overset-mesh strategy with a VOF free-surface formulation to simulate the steady turning motion of a near-surface submarine, and quantified the disturbances induced by the free surface on turning performance at different submergence depths. Guo et al. (Guo et al., 2024)conducted a similar investigation of a submarine executing a steady turning maneuver in the vicinity of the free surface, with particular emphasis on quantifying the influence of free-surface effects on turning performance. Kim (Kim, 2017) examined Zigzag maneuvering responses under two rudder-angle settings (20/20 and 30/30); compared with experimental measurements, the CFD predictions showed generally good agreement, although noticeable deviations in yaw angle and trajectory accumulated during long-duration zigzag maneuvers. Han et al. (Han et al., 2021) proposed an overset-mesh-based methodology to model autopilot-controlled maneuvering of an X-configured submarine and its 6-DOF motions, and conducted deep-water turning simulations for both port and starboard 20° rudder commands. The predicted turning trajectories, maneuvering indices, and hydrodynamic forces and moments were validated against experimental data, and the same framework was further applied to investigate port and starboard spatial spiral motions of the Joubert BB2 configuration. Zhou et al. (Han et al., 2021) performed numerical simulations of the Space Spiral Maneuver and the vertical Zigzag maneuvering motion, providing a detailed assessment of the associated hydrodynamic loads and vehicle-attitude evolution throughout the maneuvers.

Although numerous studies have performed CFD-based simulations of complex submarine maneuvering motions, the considered maneuvers are predominantly confined to the horizontal plane, whereas numerical investigations of fully three-dimensional spatial maneuvering remain scarce. Therefore, this paper proposes a numerical simulation method for three-dimensional spatial maneuvering of submarines, aiming to fill the research gap in the analysis of three-dimensional maneuvering and corresponding hydrodynamic performances.

In this study, the Joubert BB2 submarine equipped with a Marine 7371R propeller is selected as the reference configuration. An overset mesh technique is employed to prescribe the motions of the submarine and its X-rudders, while a sliding mesh approach is adopted to model propeller rotation. An autopilot based on a PD controller is implemented to regulate the vehicle attitude automatically, and the turbulent flow is resolved by solving the Reynolds-averaged Navier–Stokes (RANS) equations closed with the SST *k-ω* turbulence model. The investigation focuses on the Joubert BB2 submarine executing a Space Spiral Maneuver, with particular attention to how variations in vertical command affect key maneuvering indices (e.g., turning radius and spiral pitch) and the associated hydrodynamic performance. The remainder of the paper is organized as follows: first, the governing equations are presented; next, the submarine model, computational domain, and boundary-condition specifications are described; then, a mesh-sensitivity analysis and method validation are conducted; finally, the numerical results are discussed and analyzed.

NUMERICAL METHODS

Governing Equation

In the present work, numerical simulations were performed using the commercial CFD software STAR-CCM+ by solving the incompressible Reynolds-averaged Navier–Stokes (RANS) equations. The RANS formulation is governed by the continuity and momentum equations, which collectively describe the underlying fluid-flow dynamics. The governing equations are given as follows:

$$\frac{\partial \bar{u}_i}{\partial x_i} = 0 \tag{1}$$

$$\frac{\partial \bar{u}_i}{\partial t} + \bar{u}_j \frac{\partial \bar{u}_i}{\partial x_j} = f_i - \frac{1}{\rho}\frac{\partial \bar{p}}{\partial x_i} + \frac{1}{\rho}\frac{\partial}{\partial x_j}\left(\mu \frac{\partial \bar{u}_j}{\partial x_j} - \rho \overline{u_i' u_j'}\right) \tag{2}$$

where $\bar{u}_i$ represents the time-averaged velocity components in the Cartesian coordinate system, with the subscript i indicating the direction in the coordinate system. u_i' is the fluctuation velocity component $\rho\overline{u_i' u_j'}$ represents the Reynolds stresses.

Turbulence Model

To achieve closure of the time-averaged Navier–Stokes equations, an appropriate turbulence model is required to represent the Reynolds-stress terms. In the present study, the shear-stress transport SST *k-ω* model proposed by Menter is adopted. The corresponding transport equations are given as follows:

$$\frac{\partial(\rho k)}{\partial t} + \frac{\partial(\rho k u_j)}{\partial x_j} = \frac{\partial}{\partial x_j}\left[\left(\mu + \frac{\mu_t}{\sigma_k}\right)\frac{\partial k}{\partial x_j}\right] + P_k - \rho\beta^* k\omega + S_k \tag{3}$$

$$\frac{\partial(\rho\omega)}{\partial t} + \frac{\partial(\rho\omega u_j)}{\partial x_j} = \frac{\partial}{\partial x_j}\left[\left(\mu + \frac{\mu_t}{\sigma_\omega}\right)\frac{\partial \omega}{\partial x_j}\right] + \rho\alpha\frac{\omega}{k}P_k - \rho\beta\omega^2 + 2(1-F_1)\rho\frac{1}{\omega}\frac{\partial k}{\partial x_j}\frac{\partial \omega}{\partial x_j} + S_\omega \tag{4}$$

where, u_j represents the time-averaged velocity components, μ_t denotes the turbulent viscosity coefficient, σ_k and σ_ω represent the turbulent Prandtl numbers associated with turbulent kinetic energy and the specific dissipation rate, respectively., P_k is the turbulent kinetic energy generation term, and $2(1-F_1)\rho\frac{1}{\omega}\frac{\partial k}{\partial x_j}\frac{\partial \omega}{\partial x_j}$ represents the cross-diffusion term.

Autopilot Controller

To enable the submarine to achieve six degrees of freedom (6-DOF) motion, during the initial self-propulsion phase, the autopilot automatically controls the X-rudders to maintain both heading and attitude. The autopilot is implemented using a Proportional-Derivative (PD) controller, where the horizontal commands are regulated based on the heading and yaw angle, while the vertical commands are regulated using depth and pitch angle. According to the predefined control algorithm, the commands are then transmitted to the four rudder planes of the X-rudder. The control law governing this system is expressed as follows (Overpelt et al.):

$$\delta_{Autopilot} = P \cdot e(t) + D\frac{de(t)}{dt} \tag{5}$$

The controller commands must be decomposed into horizontal and vertical components:

$$\delta_H(t) = P_y e_y(t) + D_y \frac{de_y(t)}{dt} + P_\varphi e_\varphi(t) + D_\varphi \frac{de_\varphi(t)}{dt} \tag{6}$$

$$\delta_V(t) = P_z e_z(t) + D_z \frac{de_z(t)}{dt} + P_\theta e_\theta(t) + D_\theta \frac{de_\theta(t)}{dt} \tag{7}$$

For the X-rudder, the rudder command is the combination of the vertical and horizontal rudder commands：

$$\delta_{SbUp} = -\delta_V + \delta_H, \quad \delta_{SbDn} = -\delta_V - \delta_H \tag{8}$$

$$\delta_{PtUp} = \delta_V + \delta_H \quad , \quad \delta_{PtDn} = \delta_V - \delta_H \tag{9}$$

NUMERICAL SETUP AND VALIDATIONS

Geometric Model

The object of study in this research is the Joubert BB2 submarine model, coupled with the Marine 7371R propeller model for its propulsion system. All related investigations are conducted based on this model's scale (scale ratio 1:18.348), with the specific key parameters summarized in Table 1. A schematic representation of the model's geometric configuration is shown in Fig. 1.

Table 1. The key parameters of the Joubert BB2

Parameters	Symbol	Value (m)
Length	L	3.826
Beam	B	0.523
Drought to sail	D_s	0.883
Drought to deck	D	0.578
Drought to propeller	D_p	0.273
Longitudinal center of gravity (from nose)	x_{CG}	1.76
Vertical center of gravity (from shaft)	z_{CG}	0.286
Roll radius of gyration	I_{xx}	0.187
Yaw radius of gyration	I_{zz}	0.955
Pitch radius of gyration	I_{yy}	0.952

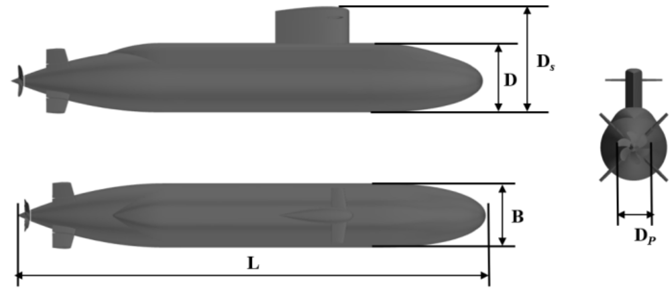

Fig. 1. Joubert BB2 submarine model coupled with Marine 7371R propeller

Computational Domain and Boundary Setting

In this study, to reduce the computational domain size required for simulating the space spiral maneuver of the submarine, a background domain follow-motion method is employed. This approach allows the background domain to move synchronously with the submarine's motion, effectively reducing the computational scale and mesh size, while enhancing computational efficiency. The computational domain is centered around the submarine, extending 2L in both the port and starboard directions as well as the aft direction, and 1L along the vertical and bow directions. In the background domain, all surfaces are treated as velocity inlets, except for the upper surface, which is designated as the pressure outlet. Fig. 2 provides a schematic representation of the computational domain defined for the study.

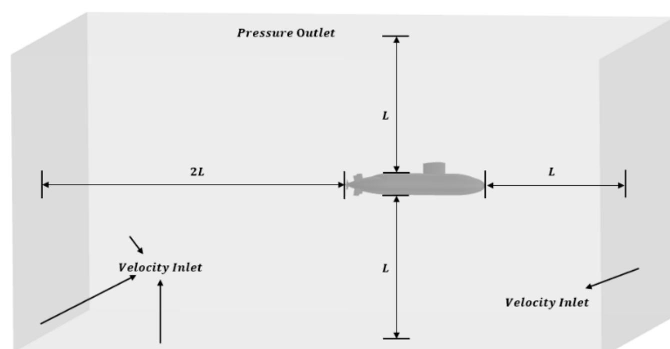

Fig. 2. Computational domain and boundary setting

Mesh Generation

As shown in Fig. 3, the mesh used in this study is depicted. An unstructured mesh is employed to discretize the surface around the Joubert BB2 model and the surrounding flow field. The background region, submarine region, and propeller region are divided using a cutting-body mesh approach, while the X-rudder region is meshed with polyhedral elements to ensure computational accuracy. The mesh in regions far from the submarine is relatively coarse to reduce computational load, while the mesh near the surface of the Joubert BB2 is refined to accurately capture the flow characteristics of the boundary layer. The overall computational domain is divided into the background domain, submarine region, X-rudder region, and propeller region using an overset mesh technique. Under the conditions of the background-domain tracking method described above, the mesh in the background domain is effectively reduced, resulting in a total of approximately 12.31 million mesh.

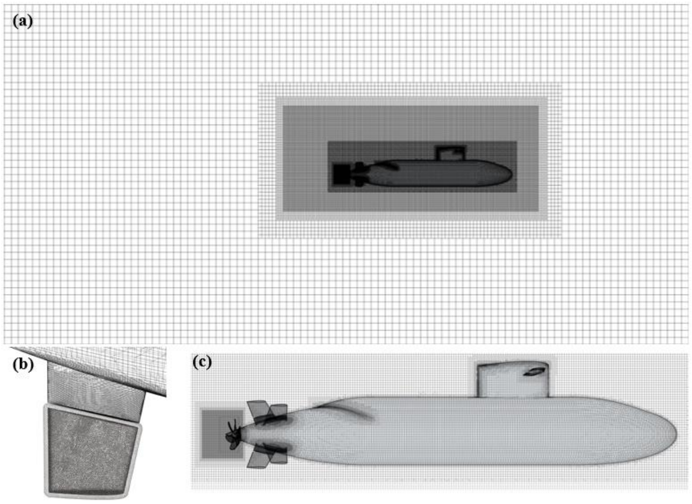

Fig. 3. The overset mesh details: (a) The mesh at the y=0 slice; (b) The overset mesh of rudders; (c) The overset mesh of the submarines.

Validation and Verification

Prior to conducting the study, a mesh convergence analysis was performed to determine an appropriate mesh cell size, with the aim of achieving an accurate numerical solution while minimizing computational costs. The meshes were categorized based on the total number of mesh cells, denoted as M_1, M_2, and M_3, where M_1 consists of 5.82 million cells, M_2 consists of 12.31 million cells, and M_3 consists of 18.64 million cells. Numerical simulations were conducted for these three mesh configurations, focusing on the convergence of the self-propulsion speed to U_0=1.2 m/s, as shown in Fig. 4. The results indicate that both the M_2 and M_3 meshes converge satisfactorily to a value near U_0. Considering both computational cost and accuracy, the M_2 mesh was selected for subsequent simulations.

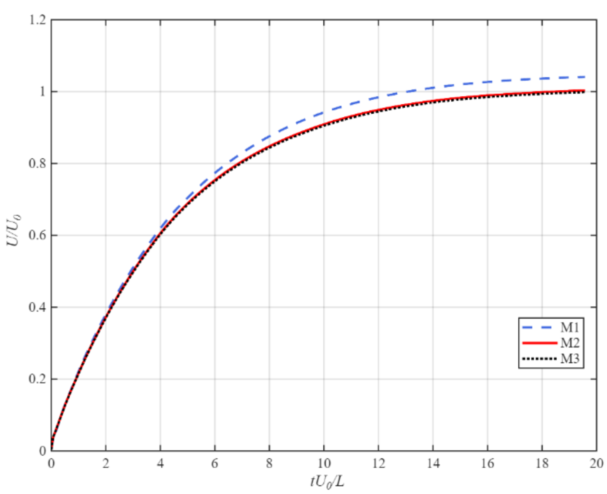

Fig. 4. The velocity of Joubert BB2 with different mesh

To validate the accuracy of the numerical simulations, the self-propulsion phase prior to the spiral maneuver is compared with experimental data from Overpelt (Overpelt et al.), as shown in Table 2. The discrepancies between the simulation results and experimental data are minimal, indicating that the CFD method can accurately replicate the actual motion.

Table 2. The results of validation

Parameters	Experiment	Present	Error
Velocity(m/s)	1.19	1.21	1.6%
Thrust(N)	26.6	27.5	3.4%

RESULTS AND DISCUSSION

This section primarily focuses on the analysis of the space spiral maneuver characteristics of the Joubert BB2 submarine. In the initial phase, the submarine performs self-propulsion until it reaches the self-propulsion point and the speed stabilizes. Once this condition is met, the autopilot is activated and executes the steering commands, transitioning the submarine into the space spiral maneuver state. This study specifically analyzes the key dynamic parameters of the submarine during the space spiral maneuver under three different vertical command conditions, with the operational parameters presented in Table 3.

Table 3. Computational cases

Case	δ_H	δ_V	Rudder Turning Rate
1	20°	5°	30.5°/s
2	20°	8°	30.5°/s
3	20°	10°	30.5°/s

Hydrodynamic Analysis

As illustrated in Fig. 5, the three-dimensional (3D) trajectories of the Joubert BB2 submarine performing the Space Spiral Maneuver are presented for all operating conditions. With increasing vertical command, the submarine exhibits a pronounced increase in lift distance during the maneuver. It should be noted that the deflection angles of the X-rudders are jointly determined by the coupled effects of the vertical and horizontal commands; consequently, even when the horizontal command is held constant, an increase in the vertical command still leads to a corresponding increase in the turning radius. The detailed values of the characteristic maneuvering parameters are provided in Table 4, in which the change in submergence depth over a 360° variation in heading angle is defined as the lift distance.

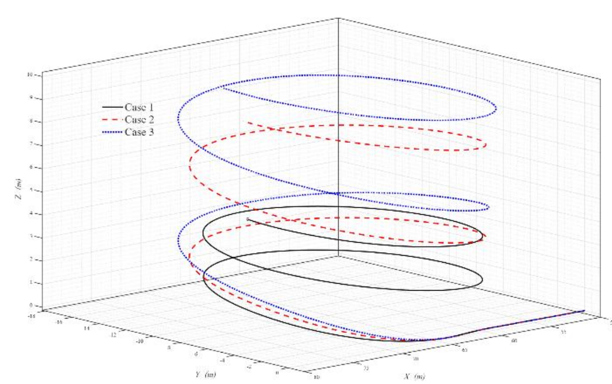

Fig. 5. Trajectory of the space spiral maneuver.

As shown in Fig. 6, the planar projected trajectories and the time histories of forward speed for the Joubert BB2 submarine during the space spiral maneuver are presented. The results indicate that, once the autopilot generates the rudder commands to initiate the spiral motion, the submarine experiences a pronounced reduction in speed. After the motion evolves toward a stable spiral state, the speed continues to decrease gradually and converges to a quasi-steady value. Moreover, the forward speed decreases with increasing vertical command: when the vertical command is 10°, the speed drops by approximately 30%, whereas reductions of about 27% and 28% are observed for vertical commands of 5° and 8°, respectively. The planar projections further show that both the tactical diameter and the turning radius increase as the vertical command increases. Specifically, the Tactical Diameter at 10° is 15.7% larger than that at 5°, while the Turning Radius increases by approximately 9.7%. In addition, once a stable Space Spiral Maneuver is established, the submarine tends to deviate further from the turning path associated with the first spiral cycle.

Table 4. Characteristic maneuvering parameters for space spiral maneuver

Case	Lift Distance / L	Tactical Diameter / L	Turning Radius / L
1	0.56	4.06	2.17
2	1.09	4.38	2.28
3	1.41	4.70	2.38

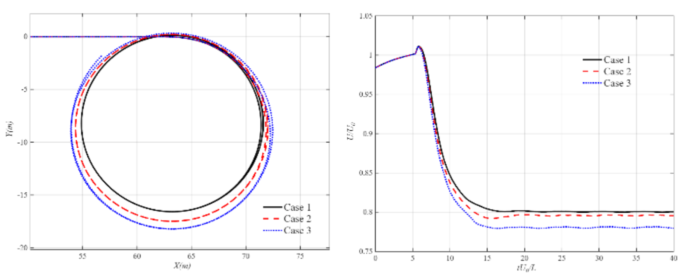

(a) Trajectory (b) Non-dimensional velocity

Fig. 6. Trajectory and Non-dimensional velocity for the space spiral maneuver.

Fig. 7 presents the time histories of the submarine's pitch and roll angles. Once the vehicle enters the space spiral maneuver state, it ascends with a bow-up attitude. The pitch angle rises rapidly to a peak immediately after the steering action and then gradually settles to a steady value. To achieve a larger lift distance during the spiral ascent, the submarine must maintain a greater bow-up attitude; accordingly, the steady-state pitch angle increases markedly with the magnitude of the vertical command. Specifically, for vertical commands of 5°, 8°, and 10°, the corresponding steady pitch angles are 11.44°, 14.24°, and 16.13°, respectively.

During the transition from self-propulsion to the space spiral maneuver, a lateral force acts on the hull and generates a lateral damping moment about the center of gravity, thereby inducing an inward heel. The roll response is characterized by a rapid increase to a peak followed by a gradual convergence to a steady value. The results further show that larger vertical commands (and hence larger lift distances) lead to reductions in both the peak and steady roll angles; for a vertical command of 10°, the steady roll angle is only 0.64°. This trend can be attributed to two mechanisms. First, an increased turning radius implies that, at comparable speeds, a smaller net lateral force is required, reducing the demand for roll-induced lateral force components and thus lowering the steady roll angle. Second, a larger pitch angle causes the rudder effectiveness and the resultant hydrodynamic force to be redistributed more toward the vertical component to realize the increased lift distance, which in turn diminishes the effective lateral component available to sustain horizontal turning.

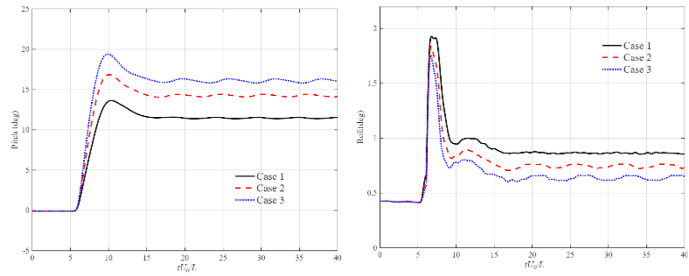

(a) Pitch (b) Roll

Fig. 7. Pitch and Roll for the space spiral maneuver.

Fig.8 shows the time histories of propeller thrust and torque for the different cases. Following the rudder action that initiates the Space Spiral Maneuver, the propeller thrust exhibits an abrupt increase and then, after a gradual adjustment, approaches a stable level during the steady spiral stage. A similar increasing trend is observed for the propeller torque. The steady-state thrust and torque levels are broadly comparable among the three cases. Notably, the case with a 5° vertical command displays smaller fluctuations and a more stable response overall, whereas the 8° and 10° cases exhibit mild oscillations in both thrust and torque.

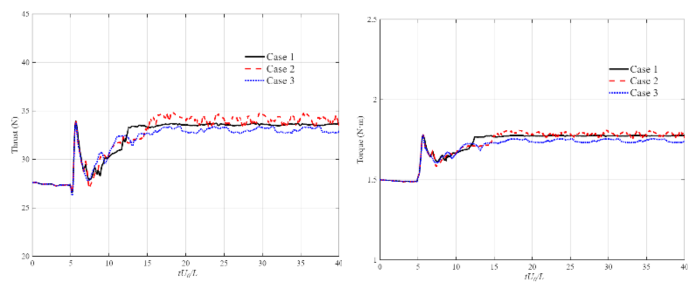

(a) Thrust (b) Torque

Fig. 8. Thrust and Torque for the space spiral maneuver.

As illustrated in Fig. 9, the axial distributions of the pressure coefficient on the upper and lower hull surfaces are quantified for the submarine during the space spiral maneuver. The three cases exhibit broadly similar pressure-distribution characteristics. In the sail region, the upper surface is dominated by a negative-pressure zone, while the lower surface features a positive-pressure zone; the resulting pressure difference generates a net hydrodynamic force acting on the forward part of the submarine. Because the axial location of this resultant is relatively upstream of the center of gravity, it produces a stern-down pitching moment, thereby promoting a bow-up tendency.

Flow Field Analysis

As shown in Fig. 10, the vortex structures and the trajectory of the Joubert BB2 submarine during the space spiral maneuver are visualized using the Q-criterion. The Q-criterion is a widely adopted method for identifying and visualizing coherent vortical structures(Hunt et al., 1988), and its mathematical definition is given in Eq. (10):

$$Q = \frac{1}{2}\left(\mathrm{P}\|\Omega\|^2 - \|S\|^2 \right) \tag{10}$$

$$\mathbf{\Omega} = \frac{1}{2}[\nabla U - (\nabla U)^T] \tag{11}$$

$$\mathbf{S} = \frac{1}{2}\left[\nabla U + (\nabla U)^T\right] \tag{12}$$

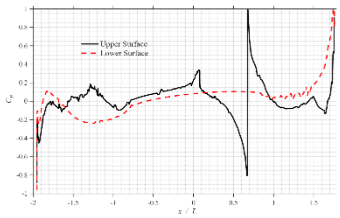

(a) Case 1

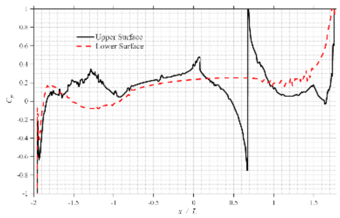

(b) Case 2

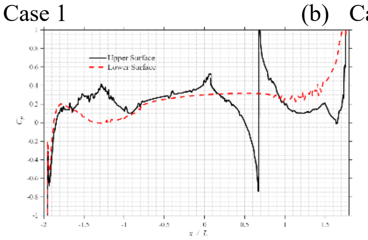

(c) Case 3

Fig. 9. Dynamic pressure coefficients of contour line along the centerline of the submarine's surface.

As shown in Fig. 10, during the spiral ascent the submarine experiences a coupled motion consisting of horizontal turning and vertical climbing, which induces pronounced three-dimensional velocity gradients in the near-body flow. In the sail and forward-hull regions, the bow-up attitude yields a relatively large effective angle of attack, causing boundary-layer separation on the leeward side and forming a concentrated vorticity region. In addition, the centrifugal effects associated with horizontal turning promote the superposition of lateral and axial flows over the mid- to aft-body, further intensifying boundary-layer shear and deformation and thereby encouraging vorticity accumulation in the downstream region of the X-rudders.

Fig.10. Vortex distribution and trajectory characteristics of the submarine space spiral maneuver.

Fig. 11 presents the submarine in a stable space spiral maneuver state, with the upper and lower hull surfaces colored by the pressure coefficient C_p. The pressure coefficient is defined as follows:

$$C_p = \frac{P - \rho g h}{\frac{1}{2}\rho U^2} \tag{13}$$

Because the space spiral maneuver involves a coupled motion of vertical lift and horizontal turning, the submarine maintains a persistent bow-up attitude once a stable spiral state is established. On the upper surface, pronounced high-pressure regions occur both upstream and downstream of the sail, whereas an evident low-pressure region develops over the aft half of the hull and in the region immediately ahead of the control surfaces. On the lower surface, a distinct low-pressure zone appears near the aft body, generating a bow-up pitching moment that balances the rudder-induced moment and the opposing sinking-related moment. This trend is consistent with the quantified axial C_p distributions shown in Fig. 9. In addition, a clear pressure gradient is observed between the starboard and port sides, producing a lateral force directed toward starboard and thereby providing the turning moment required for a starboard spiral.

From Case 1 to Case 3, the magnitude of the high-pressure region on the lower surface of the submarine increases markedly, indicating that a larger vertical command enhances lift and further amplifies the bow-up attitude. In Case 3, the high-pressure region near the stern becomes more localized, suggesting that an increased vertical command leads to a higher effective angle of attack of the aft control surfaces, thereby strengthening the pressure loading on the rudders. This enhanced rudder loading contributes to balancing the forward lift-induced pitching moment and maintaining the stability of the spiral trajectory.

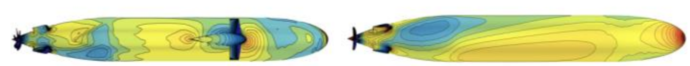

(a) Case 1

(b) Case 2

(c) Case 3

Fig.11. Dynamic pressure distribution on the upper and lower surface of submarines at the space spiral maneuver.

Fig. 12 illustrates the axial-velocity distributions on the mid-longitudinal and mid-transverse planes after the submarine has reached a stable Space Spiral Maneuver state. The contour plot clearly reflects the bow-up attitude in the vertical plane and the turning motion in the horizontal plane during the maneuver.

In addition, the blockage effects of the bow and the sail induce pronounced flow diversion, resulting in noticeable local velocity deficits in the vicinity of the bow and in the regions immediately upstream and downstream of the sail. Compared with the propeller wake under self-propulsion in straight motion, the wake field in the spiral maneuver is influenced by the coupled effects of hull inclination and aft-control-surface deflection, leading to reduced wake uniformity relative to the self-propulsion condition. Moreover, from Case 1 to Case 3, the bow-up attitude increases progressively, consistent with the corresponding monotonic increase in lift distance during the spiral motion.

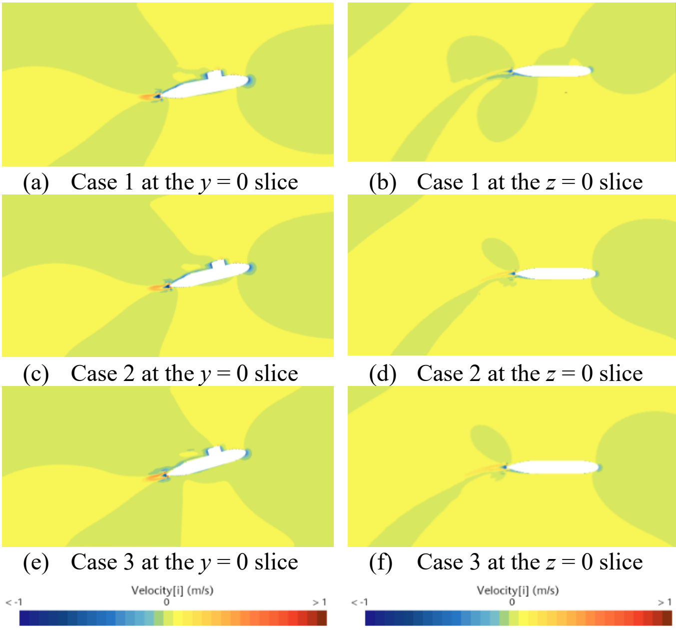

(a) Case 1 at the $y = 0$ slice (b) Case 1 at the $z = 0$ slice
(c) Case 2 at the $y = 0$ slice (d) Case 2 at the $z = 0$ slice
(e) Case 3 at the $y = 0$ slice (f) Case 3 at the $z = 0$ slice

Fig.12. Velocity field of the submarine space spiral maneuver.

CONCLUSIONS

A numerical framework for simulating a submarine executing the Space Spiral Maneuver was developed in the commercial CFD package STAR-CCM+ using an overset mesh methodology. Simulations were then carried out for the Joubert BB2 submarine in deep water under different steering commands to evaluate the hydrodynamic loads and flow-field characteristics associated with the maneuver. Based on the analysis of the computed results, the main findings can be summarized as follows:

(a) A CFD-based approach was established for investigating the Space Spiral Maneuver. The method employs an overset mesh to prescribe the motions of the submarine and its four control surfaces (X-rudders), and a sliding mesh to model propeller rotation. An autopilot strategy is implemented to regulate the horizontal and vertical attitude errors during the initial self-propulsion stage. Validation against experimental measurements under matching conditions yields a speed discrepancy of 1.6% and a thrust discrepancy of 3.4%, demonstrating the reliability of the proposed methodology.

(b) With increasing vertical command, the submarine exhibits a marked increase in pitch angle during the Space Spiral Maneuver, which in turn leads to a pronounced increase in lift distance. Meanwhile, the deflections of the X-rudders are governed by the coupled effects of the vertical and horizontal commands; consequently, even when the horizontal command is kept unchanged, a larger vertical command still results in a concomitant increase in turning radius.

(c) In the stable spiral state, high-pressure regions are observed on the upper surface upstream and downstream of the sail, whereas distinct low-pressure regions develop over the aft half of the hull and in the area immediately ahead of the control surfaces. On the lower surface, a pronounced low-pressure zone near the aft body generates a bow-up pitching moment, helping the submarine maintain a bow-up attitude. A larger vertical command substantially amplifies the high-pressure magnitude on the lower surface, indicating that the vertical command increases lift and further enhances the bow-up attitude.

ACKNOWLEDGEMENTS

This work is supported by National Natural Science Foundation of China (Nos. 52571360 and 52131102), to which the authors are most grateful.

REFERENCES

Cao, L, Gao, G, Guo, E, and Wan, D (2023). “Hydrodynamic performances and wakes induced by a generic submarine operating near the free surface in continuously stratified fluid,” *J Hydrodyn*, 35(3), 396–406.

Carrica, PM, Kerkvliet, M, Quadvlieg, F, and Martin, JE (2021). “CFD Simulations and Experiments of a Submarine in Turn, Zigzag, and Surfacing Maneuvers,” *J Ship Res*, 65(04), 293–308.

Chase, N. (2012). “Simulations of the DARPA Suboff submarine including self-propulsion with the E 1619 propeller.,”

Chen, M, Zhang, N, Zheng, W, and Li, Y (2023). “Numerical simulation of near-surface turn maneuver of a generic submarine,” *Ocean Eng*, 287, 115835.

Dogrul, A, Sezen, S, Delen, C, and Bal, S (2017). “Self-propulsion simulation of DARPA suboff: 17th International Congress of the International Maritime Association of the Mediterranean,” *Dev Marit Transp Harvest Sea Resour*,.

Fossen, TI, and Blanke, M (2000). “Nonlinear output feedback control of underwater vehicle propellers using feedback form estimated axial flow velocity,” *IEEE J Ocean Eng*, 25(2), 241–255.

Guo, E, Wang, Y, Cao, L, and Wan, D (2024). “Numerical investigation on steady turning motion of a generic submarine near the free surface,” *Ocean Eng*, 313, 119375.

Han, K, Cheng, X, Liu, Z, Huang, C, Chang, H, Yao, J, and Tan, K (2021). “Six-DOF CFD Simulations of Underwater Vehicle Operating Underwater Turning Maneuvers,” *J Mar Sci Eng*, 9(12), 1451.

Hunt, JCR, Wray, AA, and Moin, P (1988). “Eddies, streams, and convergence zones in turbulent flows.,”

Kim, H (2017) “Six-DOF Motion Response and Manoeuvring Simulation of an Underwater Vehicle.,”

Lin, K, Ye, J, and Liang, Q (2023). “Experimental Study on the Flow Field, Force, and Moment Measurements of Submarines with Different Stern Control Surfaces,” *J Mar Sci Eng*, 11(11).

Liu, H.L., Huang, T.T. (1990). “Summary of DARPA SUBOFF experimental program data.,”

Lungu, A (2022). “A DES-based study of the flow around the self-propelled DARPA Suboff working in deep immersion and beneath the free-surface,” *Ocean Eng*, 244, 110358.

Overpelt, B, Nienhuis, B, and Anderson, B (2015). “Free Running Manoeuvring Model Tests On A Modern Generic SSK Class Submarine (BB2).,”

Özden, YA, Özden, MC, Demir, E, and Kurdoğlu†, S (2019). “Experimental and Numerical Investigation of DARPA Suboff Submarine Propelled with INSEAN E1619 Propeller for Self-Propulsion.,” *J Ship Res*, 63(4), 235–250.